Journal of Solid State Chemistry 309 (2022) 122961

Contents lists available at ScienceDirect

Journal of Solid State Chemistry

journal homepage: www.elsevier.com/locate/jssc

Electrical properties of ceramics based on Ag_7TS_5I (T = Si, Ge) solid electrolytes

I.P. Studenyak [a], A.I. Pogodin [a,*], I.A. Shender [a], V.I. Studenyak [a], M.J. Filep [a,b], O.I. Symkanych [a], O.P. Kokhan [a], P. Kúš [c]

[a] Uzhhorod National University, Pidgirna St. 46, Uzhhorod, 88000, Ukraine
[b] Ferenc Rákóczi II Transcarpathian Hungarian Institute, Kossuth Sq. 6, Beregovo, 90200, Ukraine
[c] Comenius University, Mlynska dolina, Bratislava, 84248, Slovakia

ARTICLE INFO

Keywords:
Argyrodites
Superionic conductor
Ceramics
Mixed conductor
Thermally activated processes

ABSTRACT

The ceramic samples based on the synthesized compounds of Ag_7TS_5I (T = Si, Ge) solid electrolytes were prepared with using of micro- and nanocrystalline powders. Structural studies of powders obtained by grinding in an agate mortar as well as in a planetary ball mill were carried out by XRD and SEM techniques. Optical microscopy was used to estimate the size of crystallites after annealing of prepared ceramics. Temperature (292–383 K) and frequency (10 Hz–2 × 10^6 Hz) dependences of total electrical conductivity of ceramic samples were investigated by impedance spectroscopy technique. Separation of electronic and ionic parts of electrical conductivity were carried out by the analysis of Nyquist plots using electrode equivalent circuits. The dependences of ionic and electronic components of the electrical conductivity on temperature and on average size of the crystallites were investigated for Ag_7TS_5I-based ceramics. The comparison of electrical parameters for Ag_7TS_5I (T = Si, Ge) crystals, composites and ceramics was performed.

1. Introduction

Recently, an active search for new materials is underway and ways to create on the basis of already known materials the effective solid-state batteries are being developed. Among them there are well-known materials such as Li^+- та Na^+-containing solid electrolytes [1–5] or Ag^+ superionic materials based on binary α-AgI [6,7] and more complex phases as Ag_4RbI_5 [8,9] and argyrodites [10–15]. Compounds with argyrodite structure are promising materials in this respect. They are known as superionic conductors, thermoelectrics and ferroics [15–19]. They are primarily characterized by high ionic conductivity and low activation energy [12–14,17]. The ionic conductivity of argyrodites is ensured by the presence of a «rigid» anionic framework and a «mobile » cationic sublattice. The mobility of cations is provided by a significant number of equivalent crystallographic positions with their partial occupancy. In the presented materials, the charge carriers are mobile monovalent cations Li^+, Cu^+, Ag^+, and a detailed description of the conduction mechanism in these materials is presented in Refs. [10,11,20,21].

Due to their properties, they can be promising for the creation of solid-state batteries, supercapacitors, and other electrochemical devices on their basis. In order to expand the areas of their practical application, the search for new materials with predictable parameters is being carried out in such ways as: (i) the synthesis of qualitatively new materials; (ii) obtaining new materials by substituting atoms in solid solutions of already known materials; (iii) production of known materials in such various forms as ceramics, composites, thin films, etc. It should be noted that the copper-containing argyrodites were prepared in different forms such as: composites, ceramics and thin films [22–25].

Superionic ceramics are those materials that can replace single crystals due to their efficiency, manufacturability and economy [26–30]. Ceramic samples based on copper-containing argyrodites began to be studied by us in Ref. [24]. In this paper, the focus is on creating a ceramic material based on silver-containing Ag_7TS_5I (T = Si, Ge) argyrodites. The electrical properties of Ag_7TS_5I (T = Si, Ge) crystals and composites based on them were studied in Refs. [21,31–36]. However, nowadays there is no information on the study of ceramics based on Ag_7TS_5I (T = Si, Ge) compounds, despite the fact that they are promising solid electrolytes.

Thus, the main aim of this work is to study technologically simple in the production superionic conductors Ag_7TS_5I (T = Si, Ge), which are

* Corresponding author.
E-mail address: artempogodin88@gmail.com (A.I. Pogodin).

https://doi.org/10.1016/j.jssc.2022.122961
Received 28 September 2021; Received in revised form 24 January 2022; Accepted 31 January 2022
Available online 2 February 2022

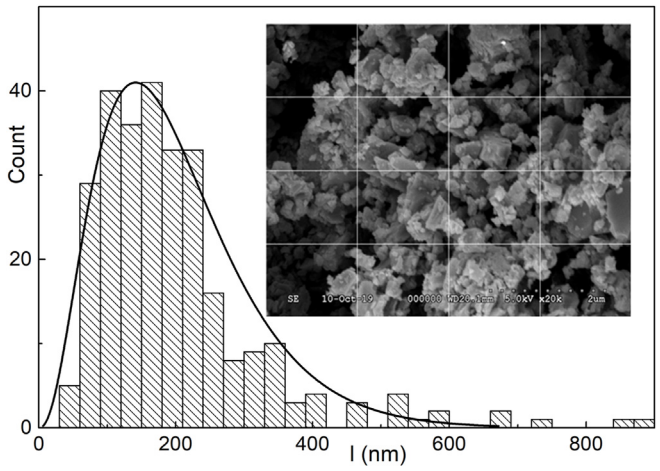

Fig. 1. Dependence of size distribution for nanocrystallites of Ag_7SiS_5I powder obtained by grinding in a planetary ball mill for 30 min. The insert shows the SEM-image of Ag_7SiS_5I nanocrystalline powder.

characterized by the optimal parameters: high ionic and low electronic conductivity. Therefore, in this work we have prepare ceramics samples based on Ag_7TS_5I (T = Si, Ge) solid electrolytes, study their structural and electrical properties (temperature and frequency dependences), separate the contributions of ionic and electronic components of electrical conductivity. Also, we establish the influence of crystallite size on the electrical parameters of obtained ceramics. Obtained electrical parameters of ceramic samples based on Ag_7TS_5I (T = Si, Ge) were compared with the same parameters of single crystals and composites.

2. Methods

Synthesis of Ag_7TS_5I (T = Si, Ge) was carried out from high purity elements: silver (99.995%), silicon (99.997%), germanium (99.999%) sulfur (99.999%), and pre-synthesized binary argentum (I) iodide in evacuated to 0.13 Pa quartz ampoules. AgI was additionally purified by directional crystallization method. First, the synthesis of Ag_7TS_5I (T = Si, Ge) bulks was performed. Ampoules with appropriate materials were slowly (rate of 100 K/h) heated to 723 K and kept for shuttering during 48 h. Further heating was performed to 1230 K at a rate of 50 K/h and was kept at this temperature for 24 h. The first temperature is required to prevent explosion of ampoules (due to high vapor pressure of sulfur) and the second one – for completeness of interaction and mixing of the components in the melt. Cooling to room temperature was performed in the oven off mode.

Powders of different dispersion were used for preparing ceramic samples: (i) microcrystalline powders obtained by grinding in an agate mortar with an average particle size of ~10–50 μm; (ii) nanocrystalline powders obtained by grinding in a planetary ball mill PQ-N04 (agate balls) for 30 min and 60 min with a speed of 200 rpm. It is shown by SEM studies that at a grinding time of 30 min the average particle size is ~150 nm while at a grinding time of 60 min the average particle size is ~100 nm. Fig. 1 shows for illustration the SEM-image and dependence of size distribution for nanocrystallites of Ag_7SiS_5I powder obtained by grinding in a planetary ball mill for 30 min.

Grinded powders of Ag_7TS_5I (T = Si, Ge) compounds were investigated using X-ray diffractometer (AXRD Benchtop powder diffractometer, Proto Manufacturing Limited) equipped with hybrid photon counting detector DECTRIS MYTHEN2 R 1D and operating with Ni filtered CuKα radiation. XRD powder patterns were collected in the Bragg-Brentano geometry (Θ/2Θ mode), angle scanning range was 10–120° 2θ with dynamic ROI (region of interest), and exposition time – 1 s per step (Fig. 2). Comparison of diffractograms (Fig. 2) indicates that the expansion of lines occurs when particle size decreases.

The obtained micro-and nanocrystalline powders was pressed at a pressure of ~400 MPa with future annealing at 973 K during 36 h (heating/cooling rate ~20 K/h). As a result, polycrystalline ceramic samples were obtained in the form of disks with a diameter of 8 and 10 mm and a thickness of 2–3 mm. The densities of pressed samples after

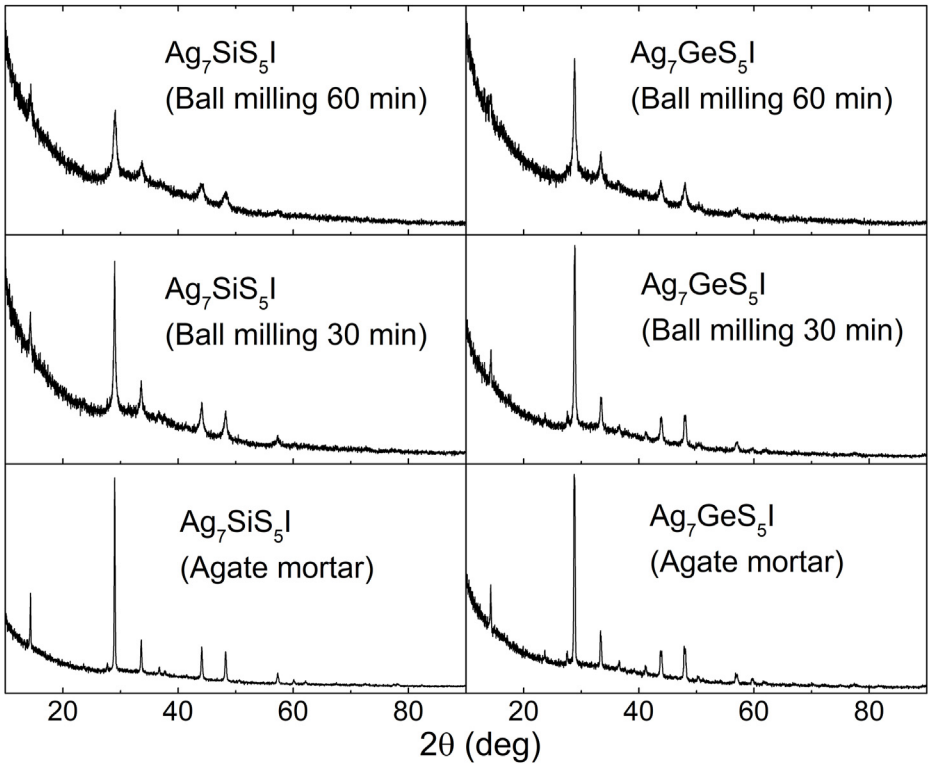

Fig. 2. Diffractograms of Ag_7SiS_5I and Ag_7GeS_5I powders obtained by grinding in agate mortar and planetary ball mill.

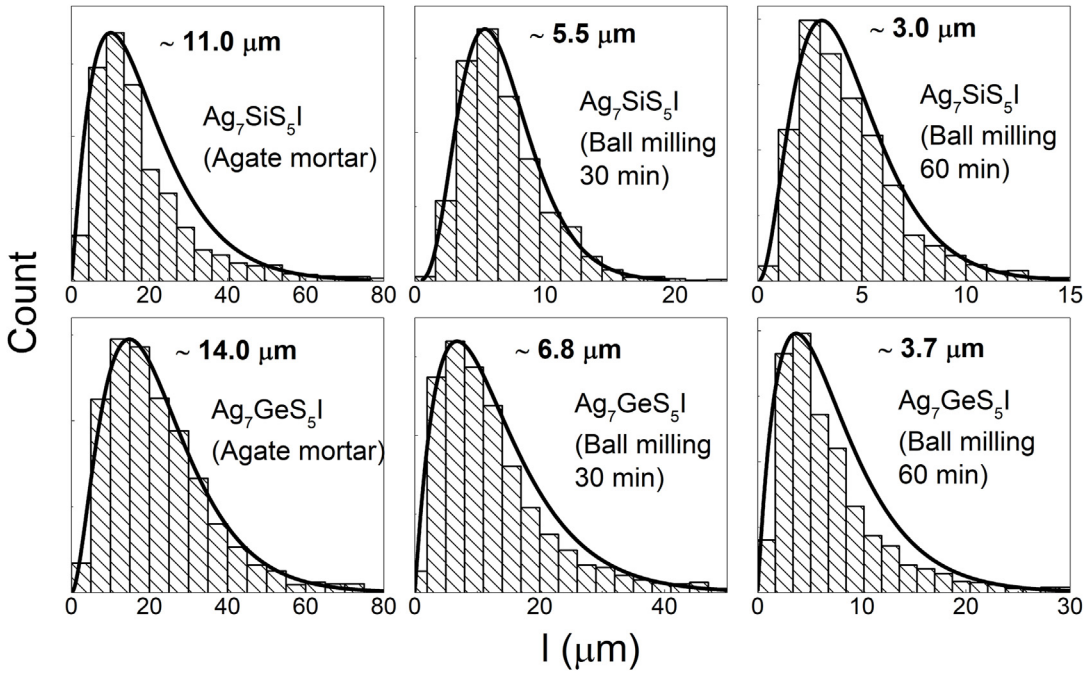

Fig. 3. Dependences of size distribution for crystallites of Ag_7SiS_5I and Ag_7GeS_5I ceramic samples, obtained from powders which were milled in agate mortar and planetary ball mill.

cold pressing and after sintering of ceramics were determined by the Archimedes method (hydrostatic weighing). After pressing, the density of disks obtained from microcrystalline powders was 91 ± 1%, while in the case of nanopowders, its value was 94 ± 1%. After annealing, the density of ceramics prepared from the both micro and nanopowders of Ag_7SiS_5I almost did not change and was 95 ± 1%, whereas in the case of Ag_7GeS_5I during recrystallization the porosity of ceramics increased as their density decreased to 83 ± 1%. The microstructural analysis of obtained ceramic samples and determination of the size of crystallites after annealing were performed by metallographic microscope METAM–R1 (Fig. 3).

According to the results of the analysis of the obtained microstructures, histograms of particle size distribution for Ag_7TS_5I (T = Si, Ge) ceramic samples, obtained from powders which were milled in agate mortar and planetary ball mill, were constructed (Fig. 3). It is established that ceramic samples obtained by sintering nanocrystalline powder are characterized by a more homogeneous microstructure, characterized by the distribution of particles in a narrower range, in contrast to the samples obtained by sintering a microcrystalline powder with a particle size of 10–50 μm. As a result of recrystallization, the average size of crystallites for ceramics prepared from microcrystalline and nanocrystalline (obtained by grinding for 30 min and 60 min) powders are ~11 μm, ~5.5 μm, ~3 μm for Ag_7SiS_5I as well as ~14 μm, ~6.8 μm, ~3.7 μm for Ag_7GeS_5I, respectively.

Electrical conductivity studies of ceramic materials based on Ag_7TS_5I (T = Si, Ge) solid electrolytes was carried out by impedance spectroscopy method [34], in frequency and temperature (292–383 K) ranges with combination of high-precision LCR meters: AT-2818 (10 Hz–3 × 10^5 Hz and Keysight E4980A (20 Hz–2 × 10^6 Hz). It should be noted that the gold contacts for measurements were applied by chemical precipitation from solutions [33].

3. Results and discussion

The measured dependences of the total electrical conductivity (σ_t) on the frequency (Fig. 4) for all investigated ceramic samples are of a typical behaviour for the solid-state electrolytes [35]: an increase in conductivity with a frequency is observed. The insert to Fig. 4 shows the dependence

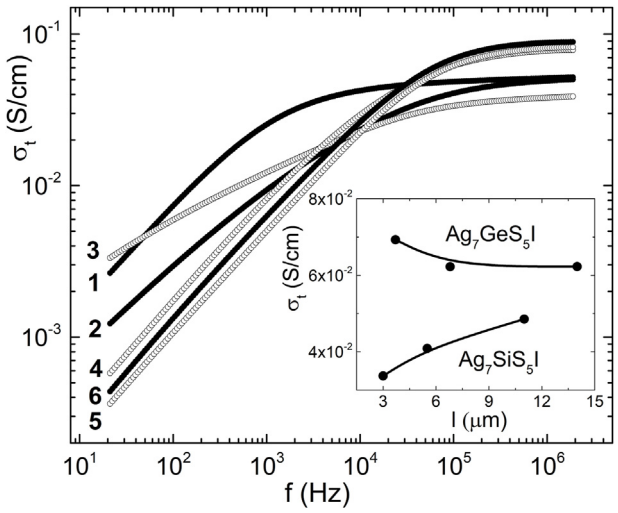

Fig. 4. Frequency dependences of total electrical conductivity at $T = 298$ K for Ag_7SiS_5I-based (1–3) and Ag_7GeS_5I-based (4–6) ceramics with different sizes of crystallites: (1) 11 μm, (2) 5.5 μm, (3) 3 μm, (4) 14 μm, (5) 6.8 μm, (6) 3.7 μm. The insert shows the dependence of the total electrical conductivity on the size of crystallites at 100 kHz for Ag_7SiS_5I-based and Ag_7GeS_5I-based ceramics.

of the σ_t on the dispersion of particles at a frequency of 100 kHz. It is revealed that at decrease of size of crystallites from 11 μm →5.5 μm→ 3 μm the decrease of total electrical conductivity for Ag_7SiS_5I-based ceramics is observed. Whereas for ceramics prepared on the basis of Ag_7GeS_5I a similar decrease in the size of the crystallites (14 μm → 6.8 μm → 3.7 μm) causes a slight increase in the total electrical conductivity. This behaviour of the total electrical conductivity may be associated with the better recrystallization ability of Ag_7GeS_5I compared to that of Ag_7SiS_5I.

Detailed studies of frequency behavior of the total electrical conductivity, its separation into ionic (σ_{ion}) and electronic (σ_{el}) parts was performed using a standard approach of electrode equivalent circuits

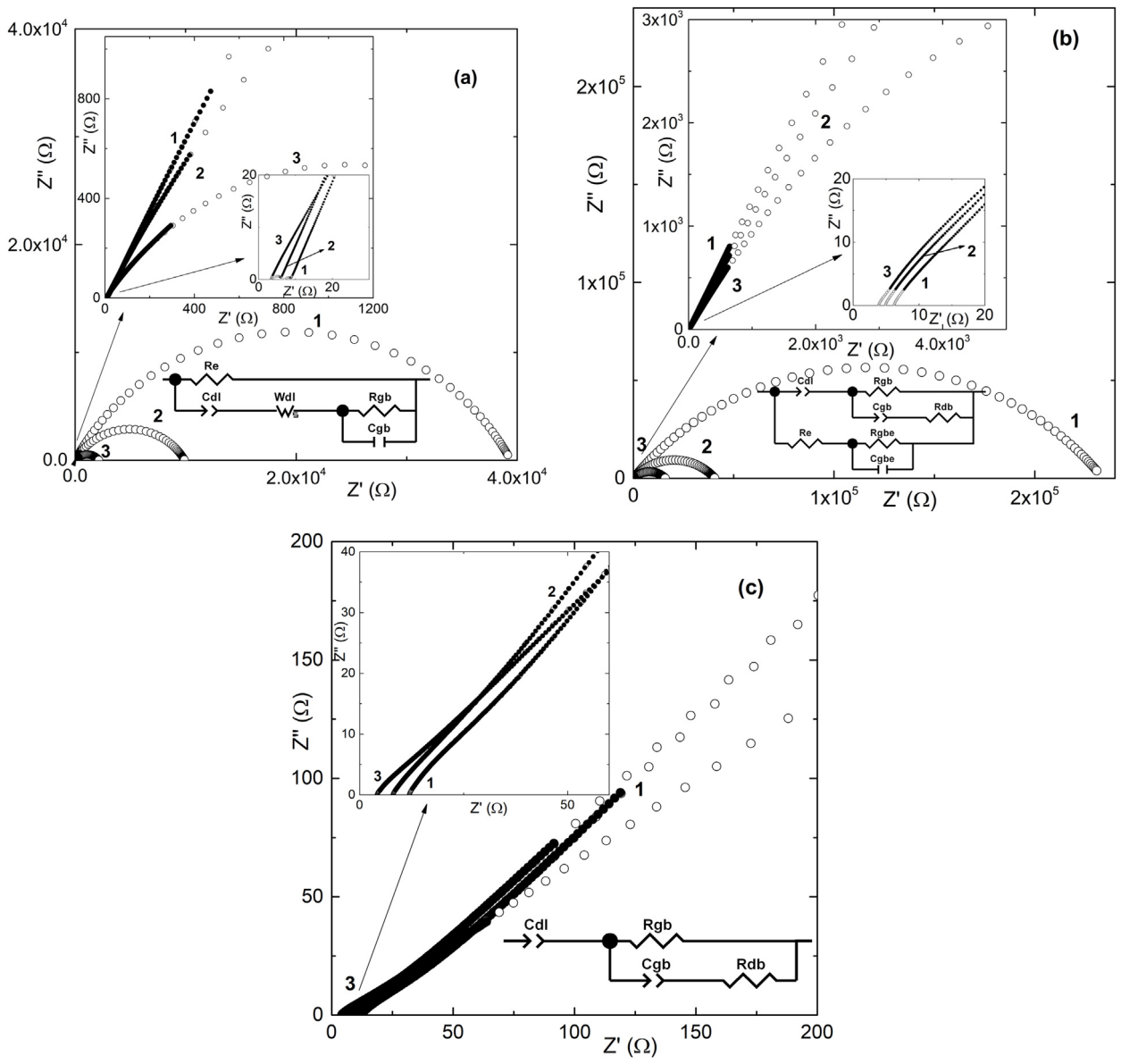

Fig. 5. EEC and Nyquist plots for Ag_7SiS_5I-based ceramics with different crystallite sizes: (a) 12 μm for temperatures (1) 298 K; (2) 323 K; (3) 373 K; (b) 5 μm for temperatures (1) 333 K; (2) 353 K; (3) 373 K; (c) 3 μm for temperatures (1) 298 K; (2) 323 K; (3) 373 K. Experimental data correspond to the solid dots, calculated data correspond to the open dots.

(EEC) [37–39] by an analysis of Nyquist plots (Z′–Z″ coordinates). The parasitic inductance of the cell (~2 × 10^{-8} H) is taken into account during the analysis of all samples.

Ceramic samples prepared on the basis of Ag_7SiS_5I are characterized by a very low value of electronic component of electrical conductivity ($\sigma_{ion}>>\sigma_{el}$), which led to the shift of the low-frequency semicircle into the low-frequency region, which is evidence of the influence of diffusion and relaxation of ionic processes. Unfortunately, due to the low-frequency limitation (10 Hz) of studies, it was not possible to determine the electronic conductivity of ceramic samples in the entire temperature range under study (for ceramics with average size of crystallites 5 μm at temperatures less than 333 K, and for ceramics with average size of crystallites 3 μm in the all studied temperature range).

For Ag_7SiS_5I ceramic samples with an average crystallite size of 11 μm and 5.5 μm (Fig. 5a and b), the presence of two semicircles is characteristic, whereas in the case of ceramics with 3 μm crystallite size (Fig. 5c) only a low-frequency part and high-frequency semicircle are observed. The high-frequency semicircles (Fig. 5a and b) are not clearly represented, so it is more correct to call them not semicircles, but high-frequency sections of the low-frequency semicircle. Low-frequency semicircles and a low-frequency part correspond to the diffusion relaxation processes at the electrode/crystal boundary. It is reflected on the EEC by the capacity of the double diffusion layer C_{dl} with serial resistance of the grain boundaries of R_{gb}, characterized by the capacity C_{gb} (for ceramic samples with an average crystallite size of 5.5 μm and 3 μm) (Fig. 5b and c), and in the case of Ag_7SiS_5I ceramic with a crystallite size of 11 μm (Fig. 5a) sequentially to the capacity of the double diffusion layer C_{dl} included is Warburg element of W_d, responsible for diffusion within the latter.

High-frequency sections for ceramic samples with an average crystallite size of 5.5 μm and 3 μm correspond to the processes determined by the resistance of intra-grain boundaries (represent the domain boundaries within an individual microcrystallite, the nature of the formation of which may be associated with the presence of small-angle boundaries formed during the recrystallization process under the influence of internal strains), which is marked by R_{db} on the EEC (Fig. 5b, c), and in the

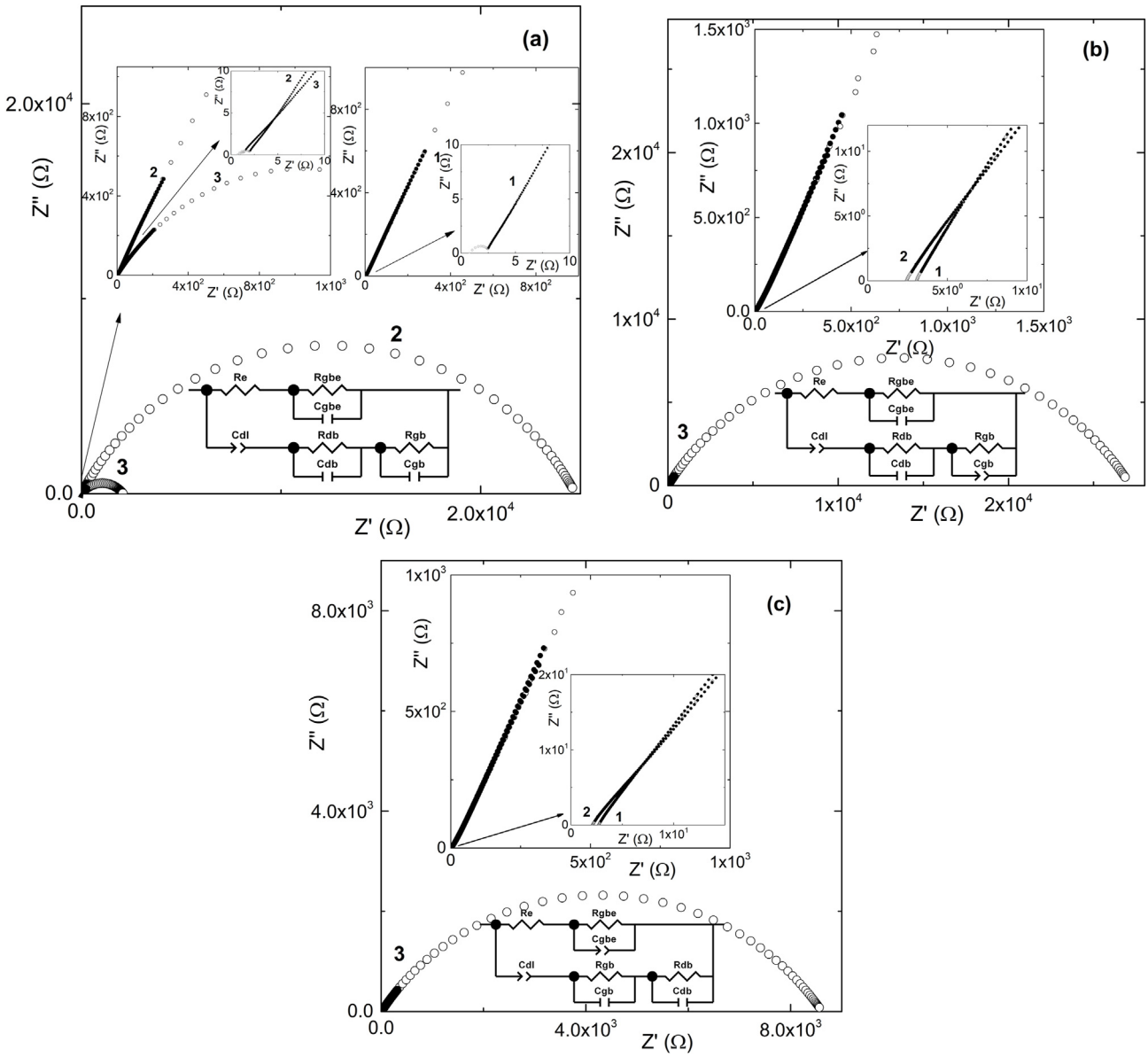

Fig. 6. EEC and Nyquist plots for Ag_7GeS_5I-based ceramics with different crystallite sizes: (a) 14 μm; (b) 6.8 μm; (c) 3.7 μm for temperatures (1) 298 K; (2) 323 K; (3) 373 K. Experimental data correspond to the solid dots, calculated data correspond to the open dots.

case of ceramics with an average crystallite size 11 μm (Fig. 5a) high-frequency sections (the end of the region of the low-frequency semicircle) is determined by the presence of resistance of the grain boundaries R_{gb}, characterized by a capacity of C_{gb}. Consequently, the ionic conductivity of Ag_7SiS_5I-based ceramics with an average crystallite size of 5.5 μm and 3 μm is determined by the sum of the resistance of grain boundaries R_{gb} and the resistance of the intra-grain boundaries R_{db}, and in the case of ceramics with average size of crystallites 11 μm (Fig. 5a) is determined by the sum of R_{gb} and the resistance limiting the ion diffusion W_R.

For ceramic samples with a crystallite size of 11 μm and 5.5 μm elements responsible for the electronic conductivity component are included on EEC parallelly to the elements responsible for ion processes. In the case of ceramics with a crystallite size of 11 μm, this is the electronic resistance R_e, and in the case of a ceramic sample with a crystallite size of 5.5 μm, the electronic resistance of the grain boundaries R_{gbe} is additionally included, which is characterized by a capacity of C_{gbe}.

Let us consider the results of temperature studies. It is shown that with increasing temperature, the increase of electronic conductivity gradually eliminates the influence of diffusion ionic processes at the boundaries of ceramics crystallites, as demonstrated by the decrease of the representation of mentioned above high-frequency section at 323 K (Fig. 5, curve 2). With further elevation of temperature up to 373 K (Fig. 5, curve 3) there is a further reduction of the influence of diffusion ionic processes, which, together with the decrease in the thickness of the double diffusion layer, and the complete disappearance of the high-frequency semicircle.

Ceramics prepared on the basis of Ag_7GeS_5I are also characterized by very low values of the electronic part of total electrical conductivity, so the limitation of the frequency range (10 Hz) also did not allow to establish its value in the following temperature ranges: 14 μm (293–303 K); 6.8 μm (293–353 K); 3.7 μm (293–333 K).

For all Ag_7GeS_5I-based ceramics in the above-mentioned temperature ranges a rectilinear section is observed in the low-frequency region on the Nyquist plots (inserts to Fig. 6). However, in the temperature ranges of 303–373 K, 353–373 K and 333–373 K, due to the increase in the value of the electronic component of electrical conductivity, this section degenerates into a low-frequency semicircle (Fig. 6). One can observe a

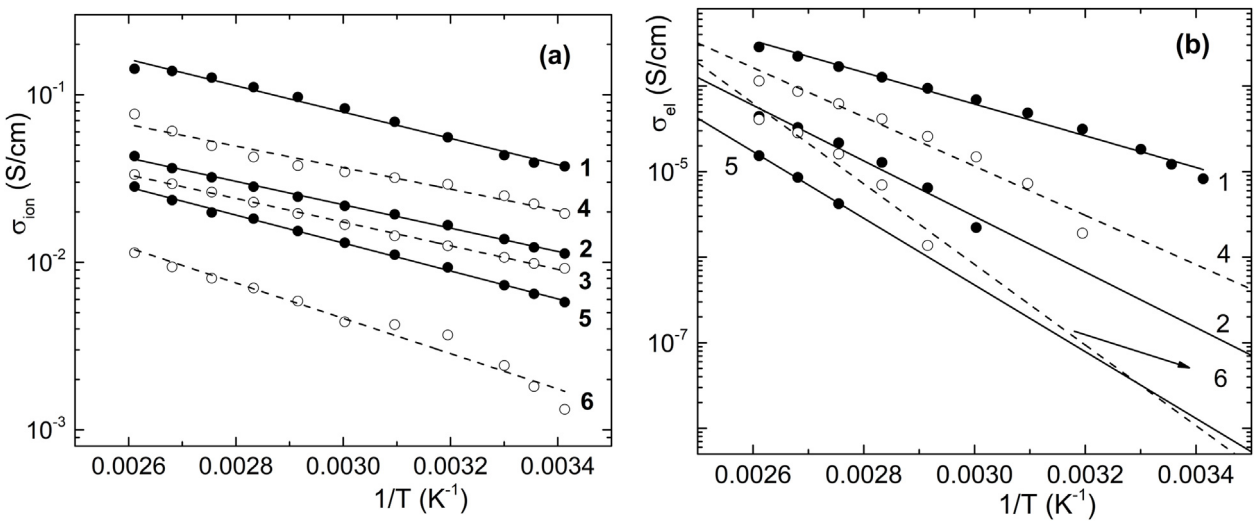

Fig. 7. Temperature dependences of ionic (a) and electronic (b) components of electrical conductivity for Ag_7SiS_5I-based (1–3) and Ag_7GeS_5I-based (4–6) ceramics with different sizes of crystallites: (1) 11 μm, (2) 5.5 μm, (3) 3 μm, (4) 14 μm, (5) 6.8 μm, (6) 3.7 μm.

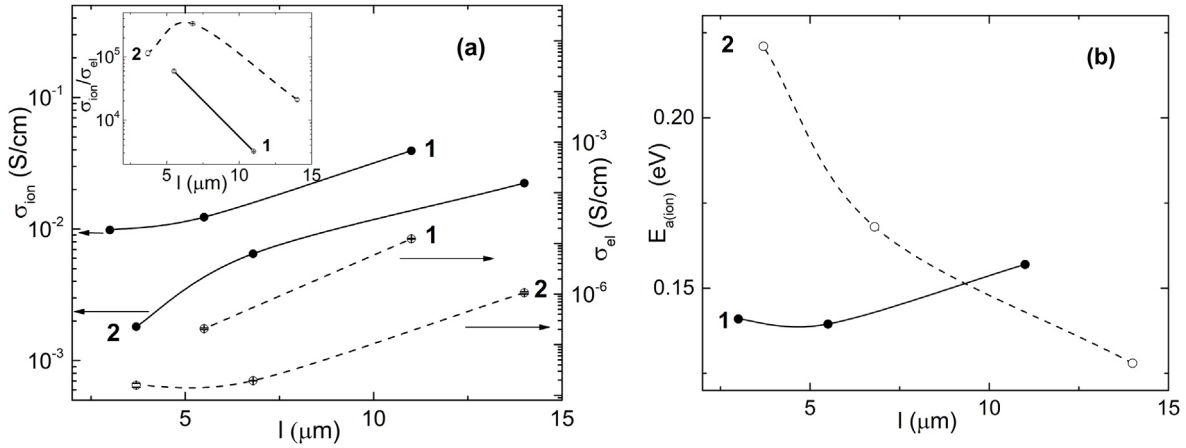

Fig. 8. (a) Dependences of ionic and electronic components of electrical conductivity at $T = 298$ K on the size of crystallites for Ag_7SiS_5I-based (1) and Ag_7GeS_5I-based (2) ceramics; the insert shows the dependence of the ratio of the conductivity components on the size of the crystallites; (b) Dependences of the activation energy of ionic component of electrical conductivity on the size of crystallites for Ag_7SiS_5I-based (1) and Ag_7GeS_5I-based (2) ceramics.

very weak high-frequency semicircle in the high-frequency region, which may be more appropriate to take as a high-frequency section. If we consider the EEC, then the low-frequency sections and/or semicircles correspond to the capacitance C_{dl}, as in the above mentioned Ag_7SiS_5I-based ceramics. Increasing the frequency (medium frequency range) allows observing the influence of the grain boundaries of ceramics, which is reflected on the EEC by the included resistance R_{gb} with parallel capacitance C_{gb} (Fig. 6) responsible for the ionic component of conductivity at the crystallite boundaries. The included resistance R_{db} and capacitance C_{db}, which determine the ionic processes at the intra-crystalline boundaries, are responsible for the high-frequency semicircles (sections) on the EEC. Thus, the ionic component of electrical conductivity of Ag_7GeS_5I ceramics is determined by the sum of $1/R_{gb}$ and $1/R_{db}$.

The elements R_e (electronic resistance) and R_{dbe}/C_{dbe} (electronic resistance of the intra-grain boundaries/capacitance), included in EEC, corresponds of electronic component of electrical conductivity. These elements contribute to the representation of both semicircles on Nyquist plots (Fig. 6). Therefore, the electronic component of the electrical conductivity of solid solutions is determined by the sum of $1/R_{dbe}$ and $1/R_e$.

The analysis of impedance spectra made it possible to investigate the temperature dependence, as well as to study the influence of the size factor on the ionic and electronic components of the conductivity of Ag_7SiS_5I-based and Ag_7GeS_5I-based ceramics.

It is established that the temperature dependences of the ionic conductivity (Fig. 7a) are linear and are described by the Arrhenius law, which confirms the thermoactivating character of conductivity. Therefore, the temperature dependences of the latter allowed determining the corresponding values of activation energy. While there is no reliability in the Arrhenius behaviour of the electronic component of electrical conductivity (Fig. 7b), due to the impossibility of its determination in the entire studied temperature range. The only exception is Ag_7SiS_5I-based ceramic with a crystallite size of 11 μm, for which the determined value of the activation energy of electronic component of electrical conductivity is 0.739 eV (Fig. 7b, curve 1). As a result, the temperature dependences of the electronic component of electrical conductivity were used only to estimate its value at a temperature of 298 K, by linearization (Fig. 7b).

Fig. 8a shows the dependences of both components of electrical conductivity on the size of crystallites in ceramic samples based on Ag_7SiS_5I (Fig. 8a, curve 1) and Ag_7GeS_5I (Fig. 8a, curve 2) solid electrolytes. It is established that the decrease in the size of crystallites leads to a monotonous reduction both ionic and electronic components of electrical conductivity, while their ratio monotonously increases, which

Table 1
Values of ionic σ_{ion} and electronic σ_{el} components of electrical conductivity as well as their ratio σ_{ion}/σ_{el} for crystal, composite and ceramic samples of Ag_7TS_5I (T = Si, Ge) solid electrolytes.

Materials	Ag_7SiS_5I			Ag_7GeS_5I		
	σ_{ion} (S/cm)	σ_{el} (S/cm)	σ_{ion}/σ_{el}	σ_{ion} (S/cm)	σ_{el} (S/cm)	σ_{ion}/σ_{el}
Crystals	8.13×10^{-3} [33]	8.32×10^{-7} [33]	9879 [33]	7.98×10^{-3} [34]	6.86×10^{-8} [34]	116292 [34]
Composites	2.96×10^{-4} [32]	2.90×10^{-5} [32]	10.2 [32]	1.60×10^{-3} [36]	3.60×10^{-9} [36]	444444 [36]
Ceramics	39.3×10^{-3} (11 μm)	$1.23\pm 0.02 \times 10^{-5}$ (11 μm)	3195± 52 (11 μm)	22.3×10^{-3} (14 μm)	$1.06\pm 0.05 \times 10^{-6}$ (14 μm)	21038± 995 (14 μm)
Ceramics	12.3×10^{-3} (5.5 μm)	$2.07\pm 0.08 \times 10^{-7}$ (5.5 μm)	59420± 2300 (5.5 μm)	6.48×10^{-3} (6.8 μm)	$1.94\pm 0.01 \times 10^{-8}$ (6.8 μm)	334021± 1722 (6.8 μm)
Ceramics	9.83×10^{-3} (3 μm)	–	–	1.81×10^{-3} (3.7 μm)	$1.58\pm 0.14 \times 10^{-8}$ (3.7 μm)	114557± 10231 (3.7 μm)

Frequency dependencies of total electrical conductivity Ag_7TS_5I (T = Si, Ge) based ceramics and dependencies of ionic part of electrical conductivity on crystallite size.

is observed for Ag_7SiS_5I-based ceramics. As the size of the crystallites decreases, there is an increase in the number of grain boundaries, which usually causes a decrease in electrical conductivity. But the studied materials Ag_7TS_5I (T = Si, Ge) belong to a mixed conductors (ion – electronic conductors), for which the dependence of the change in the conductivity components, depending on the size of the crystallites, is not proportional (the changes aren't equivalent). It is shown that microcrystalline ceramics have the highest values of ionic conductivity, but the electronic component is also quite high. At the same time, the value of ionic conductivity of ceramics prepared from nanopowders is not inferior to the previous one, but has a very low electronic component. In Ag_7GeS_5I-based ceramics (insert to Fig. 8a, curve 2), a significant decrease in the electronic component of electrical conductivity and a slight decrease in the ionic component led to a maximum at the corresponding ratio of ~3×10^5 times.

A slight decrease in activation energy with decreasing crystallite size is observed on the dependence of the activation energy of ionic conductivity on the average size of crystallites (Fig. 8b, curve 1) for Ag_7SiS_5I-based ceramics. At the same time, the activation energy of ionic conductivity for Ag_7GeS_5I-based ceramics increases with decreasing the crystallite size (Fig. 8b, curve 2).

As it shown in Refs. [40,41], the combination of the micro- and macro-defects (inevitably formed in recrystallization process during annealing) and disordered crystal structure of Ag_7TS_5I (T = Si, Ge) compounds (presence of a mobile cationic sublattice and rigid anionic frame) leads to a change in the appearance of the dependences of the Nyquist plots for samples of different dispersion (Figs. 5 and 6) and causes the corresponding behavior of the total electrical conductivity (Fig. 4), its ionic and electronic components (Fig. 8a), and is determining for the nature of thermoactivation behavior (Fig. 7a and b) of ceramic materials based on Ag_7TS_5I (T = Si, Ge) compounds.

During the process of cold pressing in the crystallites mechanical stresses appears. These stresses will be greater the larger are the size of the crystallites in the initial powders from which the pressing was performed. During the annealing process, the mechanical stresses decrease, but the result is the formation of defects within the microcrystallites, and a further solid-phase diffusion causes the process of recrystallization (aggregation of crystallites). This causes the "movement" of defects from the "center" of the original crystallites to their boundaries, i.e. a larger but strongly defective crystallite is formed. It is already known that the presence of defects can lead to an increase in the ionic component of electrical conductivity, which is possible and occurs in this case. Perhaps that in the case of Ag_7SiS_5I and Ag_7GeS_5I there is a fact that the influence of defects that promote ion transport prevail the influence of the boundaries of "recrystallized crystallites" (ceramics made of microcrystalline powders). While for ceramics made of nanocrystalline powders, for which the number of defects is smaller from the beginning, the increasing number of grain/intra-grain boundaries is the predominant factor.

Finally, let us compare the values of ionic and electronic conductivities, as well as their ratio for crystal, composite and ceramic samples of Ag_7TS_5I (T = Si, Ge) (Table 1). It is seen that the ionic conductivity of all Ag_7SiS_5I-based ceramics is greater than that of crystal and composite ones. However, in the case of Ag_7GeS_5I-based ceramics, more in comparison with the crystal, the value of the ionic component of electrical conductivity is observed only for the material with an average crystallite size of 14 μm. Despite the fact that in ceramic samples the ionic conductivity decreases with decreasing crystallite size, however, due to a more significant reduction in electronic conductivity, the ratio σ_{ion}/σ_{el} increases and for a ceramic sample with an average crystallite size of 5.5 μm (Ag_7SiS_5I) and 6.8 μm (Ag_7GeS_5I) becomes larger than for the crystals.

Thus, the carried out comparative analysis testifies to the prospects of application of superionic ceramics instead of crystals and composites in devices of solid-state ionics due to their greater manufacturability and economy.

4. Conclusions

The synthesis of Ag_7TS_5I (T = Si, Ge) solid electrolytes as well as preparation of ceramic samples on their base were carried out. For the ceramic samples preparation, the micro- and nanocrystalline powders obtained by grinding in an agate mortar as well as in a planetary ball mill were used. The structural studies of micro- and nanocrystalline powders were performed by XRD and SEM techniques, while the annealed ceramic discs were investigated by optical microscopy method. The frequency dependences of total electrical conductivity of ceramic samples were measured applying a two-electrode technique on gold contacts by impedance spectroscopy method in temperature interval 292–383 K.

The frequency dependences of the total electrical conductivity were analysed by the Nyquist plots by electrode equivalent circuits approach. As a result, total electrical conductivity of Ag_7TS_5I-based ceramics was separated into ionic and electronic components. It is revealed that the decrease in the size of crystallites leads to monotonous reduction of ionic conductivity. Established that the dependences of ionic and electronic components in Arrhenius coordinates are linear, which confirms the thermoactivating character of electrical conductivity.

The comparative analysis of electrical parameters for crystal, composite and ceramic samples of Ag_7TS_5I (T = Si, Ge) solid electrolytes has shown that the ceramics more applicable than the crystals and composites for developing of solid-state batteries not only due to the high ionic conductivity, but due to their greater manufacturability and economy.

CRediT authorship contribution statement

I.P. Studenyak: Supervision. **A.I. Pogodin:** Visualization, Investigation, Writing – original draft. **I.A. Shender:** Investigation, Software, Validation. **V.I. Studenyak:** Software, Writing – original draft. **M.J. Filep:** Data curation, Visualization, Writing – original draft. **O.I. Symkanych:** Investigation, Methodology. **O.P. Kokhan:** Conceptualization, Methodology. **P. Kúš:** Writing – review & editing.

Declaration of competing interest

The authors declare that they have no known competing financial interests or personal relationships that could have appeared to influence the work reported in this paper.

References

[1] C. Zhao, L. Liu, X. Qi, Y. Lu, F. Wu, J. Zhao, Y. Yu, Y.-S. Hu, L. Chen, Solid-state sodium batteries, Adv. Energy Mater. 8 (2018) 1703012, https://doi.org/10.1002/aenm.201703012.

[2] Y. Wang, S. Song, C. Xu, N. Hu, J. Molenda, L. Lu, Development of solid-state electrolytes for sodium-ion battery – a short review, Nano Mater. Sci. 1 (2019) 91–100, https://doi.org/10.1016/j.nanoms.2019.02.007.

[3] Z. Wu, Z. Xie, A. Yoshida, Z. Wang, X. Hao, A. Abudula, G. Guan, Utmost limits of various solid electrolytes in all-solid-state lithium batteries: a critical review, Renew. Sustain. Energy Rev. 109 (2019) 367–385, https://doi.org/10.1016/j.rser.2019.04.035.

[4] I.X. Bai, Y. Duan, W. Zhuang, R. Yang, J. Wang, Research progress in Li-argyrodite-based solidstate electrolytes, J. Mater. Chem. A. 8 (2020) 25663–25686, https://doi.org/10.1039/D0TA08472G.

[5] Z. Zhang, L. Zhang, Y. Liu, C. Yu, X. Yan, B. Xu, L. Wang, ynthesis and characterization of argyrodite solid electrolytes for all-solid-state li-ion batteries, in: S, vol. 747, 2018, pp. 227–235, https://doi.org/10.1016/j.jallcom.2018.03.027.

[6] T. Yamamoto, M. Maesato, N. Hirao, S.I. Kawaguchi, S. Kawaguchi, Y. Ohishi, Y. Kubota, H. Kobayashi, H. Kitagawa, The room-temperature superionic conductivity of silver iodide nanoparticles under pressure, J. Am. Chem. Soc. 139 (2017) 1392–1395, https://doi.org/10.1021/jacs.6b11379.

[7] R. Makiura, T. Yonemura, T. Yamada, M. Yamauchi, R. Ikeda, H. Kitagawa, K. i Kato, M. Takata, Size-controlled stabilization of the superionic phase to room temperature in polymer-coated AgI nanoparticles, Nat. Mater. 8 (2009) 476–480, https://doi.org/10.1038/nmat2449.

[8] A. Pinkowski, T. Chierchie, W.J. Lorenz, Low-temperature ion conductivity of $RbAg_4I_5$, J. Electroanal. Chem. Interfacial Electrochem. 285 (1990) 241–248, https://doi.org/10.1016/0022-0728(90)87124-3.

[9] K. Funke, R.D. Banhatti, D. Wilmer, R. Dinnebier, A. Fitch, M. Jansen, Low-temperature phases of rubidium silver iodide:crystal structures and dynamics of the mobile silver ions, J. Phys. Chem. 110 (2006) 3010–3016, https://doi.org/10.1021/jp054807v.

[10] W.F. Kuhs, R. Nitsche, K. Scheunemann, The argyrodites – a new family of the tetrahedrally close-packed structures, Mater. Res. Bull. 14 (1979) 241–248, https://doi.org/10.1016/0025-5408(79)90125-9.

[11] T. Nilges, A. Pfitzner, A structural differentiation of quaternary copper argyrodites: structure – property relations of high temperature ion conductors, Z. Kristallogr. 220 (2005) 281–294, https://doi.org/10.1524/zkri.220.2.281.59142.

[12] H.-J. Deiseroth, S.-T. Kong, H. Eckert, J. Vannahme, C. Reiner, T. Zaiß, M. Schlosser, Li_6PS_5X: a class of crystalline Li-rich solids with an unusually high Li^+ mobility, Angew. Chem. Int. Ed. 47 (2008) 755–758, https://doi.org/10.1002/anie.200703900.

[13] L. Zhou, A. Assoud, Q. Zhang, X. Wu, L.F. Nazar, New family of argyrodite thioantimonate lithium superionic conductors, J. Am. Chem. Soc. 141 (2019) 19002−, https://doi.org/10.1021/jacs.9b08357, 19013.

[14] W.D. Jung, J.-S. Kim, S. Choi, S. Kim, M. Jeon, H.-G. Jung, K.Y. Chung, J.-H. Lee, B.-K. Kim, J.-H. Lee, H. Kim, Superionic halogen-rich Li-argyrodites using in situ nanocrystal nucleation and rapid crystal growth, Nano Lett. 20 (2020) 2303–2309, https://doi.org/10.1021/acs.nanolett.9b04597.

[15] M.A. Kraft, S. Ohno, T. Zinkevich, R. Koerver, S.P. Culver, T. Fuchs, A. Senyshyn, S. Indris, B.J. Morgan, W.G. Zeier, Inducing high ionic conductivity in the lithium superionic argyrodites $Li_{6+x}P_{1-x}Ge_xS_5I$ for all-solid-state batteries, J. Am. Chem. Soc. 140 (2018) 16330–16339, https://doi.org/10.1021/jacs.8b10282.

[16] I.P. Studenyak, M. Kranjčec, GySh Kovacs, V.V. Panko, YuM. Azhnyuk, I.D. Desnica, O.M. Borets, YuV. Voroshilov, Fundamental optical absorption edge and exciton-phonon interaction in of Cu_6PS_5Br superionic ferroelastic, Mater. Sci. Eng. B52 (1998) 202–207, https://doi.org/10.1016/S0921-5107(97)00278-X.

[17] I.P. Studenyak, M. Kranjčec, M.V. Kurik, Urbach rule and disordering processes in $Cu_6P(S_{1-x}Se_x)_5Br_{1-y}I_y$ superionic conductors, J. Phys. Chem. Solid. 67 (2006) 807–817, https://doi.org/10.1016/j.jpcs.2005.10.184.

[18] B. Jiang, P. Qiu, E. Eikeland, H. Chen, Q. Song, D. Ren, T. Zhang, J. Yang, B. Brummerstedt Iversen, X. Shi, L. Chen, Cu_8GeSe_6-based thermoelectric materials with an argyrodite structure, J. Mater. Chem. C 5 (2017) 943–952, https://doi.org/10.1039/C6TC05068A.

[19] X. Shen, C.-C. Yang, Y. Liu, G. Wang, H. Tan, Y.-H. Tung, G. Wang, X. Lu, J. He, X. Zhou, High-temperature structural and thermoelectric study of argyrodite Ag_8GeSe_6, ACS Appl. Mater. Interfaces 11 (2019) 2168–2176, https://doi.org/10.1021/acsami.8b19819.

[20] A.R. Stamminger, B. Ziebarth, M. Mrovec, T. Hammerschmidt, R. Drautz, Ionic conductivity and its dependence on structural disorder in halogenated argyrodites Li_6PS_5X (X = Br, Cl, I), Chem. Mater. 31 (2019) 8673–8678, https://doi.org/10.1021/acs.chemmater.9b0204.

[21] I.P. Studenyak, A.I. Pogodin, M.J. Filep, O.I. Symkanych, T.Y. Babuka, O.P. Kokhan, P. Kúš, Influence of heterovalent cationic substitution on electrical properties of $Ag_{6+x}(P_{1-x}Ge_x)S_5I$ solid solutions, J. Alloys Compd. 873 (2021) 159784, https://doi.org/10.1016/j.jallcom.2021.159784.

[22] A.F. Orliukas, E. Kazakevicius, A. Kezionis, T. Salkus, I.P. Studenyak, R.Yu Buchuk, I.P. Prits, V.V. Panko, Preparation, electric conductivity and dielectrical properties of Cu_6PS_5I-based superionic composites, Solid State Ionics 180 (2009) 183–186, https://doi.org/10.1016/j.ssi.2008.12.005.

[23] I.P. Studenyak, V.Yu Izai, V.I. Studenyak, O.V. Kovalchuk, T.M. Kovalchuk, P. Kopčanský, M. Timko, N. Tomašovičová, V. Zavisova, J. Miskuf, I.V. Oleinikova, Influence of Cu_6PS_5I superionic nanoparticles on the dielectric properties of 6CB liquid crystal, Liq. Cryst. 44 (2017) 897–903, https://doi.org/10.1080/02678292.2016.1254288.

[24] T. Šalkus, E. Kazakevičius, J. Banys, M. Kranjčec, A.A. Chomolyak, YuYu Neimet, I.P. Studenyak, Influence of grain size effect on electrical properties of Cu_6PS_5I superionic ceramics, Solid State Ionics 262 (2014) 597–600, https://doi.org/10.1016/j.ssi.2013.10.040.

[25] I.P. Studenyak, M. Kranjčec, V.Yu Izai, A.A. Chomolyak, M. Vorohta, V. Matolin, C. Cserhati, S. Kökényesi, Structural and temperature-related disordering studies of Cu_6PS_5I amorphous thin films, Thin Solid Films 520 (2012) 1729–1733, https://doi.org/10.1016/j.tsf.2011.08.043.

[26] J.W. Fergus, Ceramic and polymeric solid electrolytes for lithium-ion batteries, J. Power Sources 195 (2010) 4554–4569, https://doi.org/10.1016/j.jpowsour.2010.01.076.

[27] A. Hayashi, K. Noi, A. Sakuda, M. Tatsumisago, Superionic glass-ceramic electrolytes for room-temperature rechargeable sodium batteries, Nat. Commun. 3 (2012) 856, https://doi.org/10.1038/ncomms1843.

[28] Z. Zhang, Q. Zhang, C. Ren, F. Luo, Q. Ma, Y.-S. Hu, Z. Zhou, H. Li, X. e Huang, L. Chen, A ceramic/polymer composite solid electrolyte for sodium batteries, J. Mater. Chem. 4 (2016) 15823–15828, https://doi.org/10.1039/C6TA07590H.

[29] K.H. Park, D.H. Kim, H. Kwak, S.H. Jung, H.-J. Lee, A. Banerjee, J.H. Lee, Y.S. Jung, Solution-derived glass-ceramic $NaI{\times}Na_3SbS_4$ superionic conductors for all-solid-state Na-ion batteries, J. Mater. Chem. 6 (2018) 17192–17200, https://doi.org/10.1039/C8TA05537H.

[30] M. Pogosova, I. Krasnikova, A. Sergeev, A. Zhugayevych, K. Stevenson, Correlating structure and transport properties in pristine and environmentally-aged superionic conductors based on $Li_{1.3}Al_{0.3}Ti_{1.7}(PO_4)_3$ ceramics, J. Power Sources 448 (2020) 227367, https://doi.org/10.1016/j.jpowsour.2019.227367.

[31] M. Laqibi, B. Cros, S. Peytavin, M. Ribes, New silver superionic conductors Ag_7XY_5Z (X = Si, Ge, Sn; Y = S, Se; Z = Cl, Br, I) – synthesis and electrical studies, Solid State Ionics 23 (1987) 21–26, https://doi.org/10.1016/0167-2738(87)90077-4.

[32] A.I. Pogodin, O.P. Kokhan, O.O. Yamkoviy, L.M. Suslikov, I.P. Studenyak, Electrical properties of composites based on solid solutions of $(Cu_{1-x}Ag_x)_7SiS_5I$ superionic conductors, vol. 45, Uzhhorod University Scientific Herald: Series Physics, 2019, pp. 19–26, https://doi.org/10.24144/2415-8038.2019.45.19-26 (in Ukrainian).

[33] I.P. Studenyak, A.I. Pogodin, V.I. Studenyak, V.Yu Izai, M.J. Filep, O.P. Kokhan, M. Kranjčec, P. Kúš, Electrical properties of copper- and silver-containing superionic $(Cu_{1-x}Ag_x)_7SiS_5I$ mixed crystals with argyrodite structure, Solid State Ionics 345 (6) (2020) 115183, https://doi.org/10.1016/j.ssi.2019.115183.

[34] A.I. Pogodin, V.I. Studenyak, M.Y. Filep, O.P. Kokhan, I.P. Studenyak, P. Kúš, Influence of cation substitution on ionic and electronic conductivity of $(Cu_{1-x}Ag_x)_7GeS_5I$ mixed crystals, Ukrainian J. Phys. 66 (2021) 341–347, https://doi.org/10.15407/ujpe66.4.341.

[35] V. Kavaliukė, T. Šalkus, S. Balčiūnas, J. Banys, A.I. Pogodin, O.P. Kokhan, I.P. Studenyak, Electrical properties of $(Cu_{1-x}Ag_x)_7GeS_5I$ crystals investigated by impedance spectroscopy, Solid State Ionics 363 (2021) 115593, https://doi.org/10.1016/j.ssi.2021.115593.

[36] V.Yu Izai, V.I. Studenyak, A.I. Pogodin, I.P. Studenyak, M. Rajňák, J. Kurimsky, M. Timko, P. Kopčanský, Electrical and dielectrical properties of composites based on $(Ag_{1-x}Cu_x)_7GeS_5I$ mixed crystals, Semiconductor Physics, Quant. Electron. Optoelectron. 21 (2018) 387–391, https://doi.org/10.15407/spqeo21.04.387.

[37] M.E. Orazem, B. Tribollet, Electrochemical Impedance Spectroscopy, John Wiley & Sons, New Jersey, 2008.

[38] A.K. Ivanov-Schitz, I.V. Murin, Solid State Ionics, vol. 1, S.-Petersburg Univ. Press, 2000 (in Russian).

[39] R.A. Huggins, Simple method to determine electronic and ionic components of the conductivity in mixed conductors: a review, Ionics 8 (2002) 300–313, https://doi.org/10.1007/BF02376083.

[40] I.P. Studenyak, A.I. Pogodin, I.A. Shender, S.M. Bereznyuk, M.J. Filep, O.P. Kokhan, P. Kúš, Preparation and electrical conductivity of $(Cu_{0.5}Ag_{0.5})_7SiS_5I$-based superionic ceramics, J. Alloys Compd. 854 (2021) 157131, https://doi.org/10.1016/j.jallcom.2020.157131.

[41] I.P. Studenyak, A.I. Pogodin, I.A. Shender, S.M. Bereznyuk, M.J. Filep, O.P. Kokhan, P. Kopčanský, Structural and impedance studies of copper-enriched $(Cu_{0.75}Ag_{0.25})_7SiS_5I$-based ceramics, Semiconductor Physics, Quant. Electron. Optoelectron. 23 (3) (2020) 260–266, https://doi.org/10.15407/spqeo23.03.260.